

## Forecasting Tropical Cyclone Turning Motion from Surrounding Wind and Temperature Fields

JOHNNY C. L. CHAN, WILLIAM M. GRAY AND STANLEY Q. KIDDER<sup>1</sup>

*Department of Atmospheric Science, Colorado State University, Fort Collins 80523*

(Manuscript received 30 July 1979, in final form 31 January 1980)

### ABSTRACT

An analysis of tropical cyclone forecast track errors shows that the largest errors are typically associated with storms undergoing turning motion. This paper presents results obtained from a composite study of tropical cyclones occurring in the West Indies during 1961–77. Storms which underwent a left or right turn or moved straight for a period of at least 36 h were studied. Wind fields at different levels in the atmosphere around these storms were investigated.

When a storm begins to turn, the environmental flow at 500 mb and the average tropospheric wind (between 200 and 900 mb) around the cyclone at 5–11° latitude radius is cyclonic for a left turning and anticyclonic for a right turning storm. At 24–36 h before a storm makes a left turn, there exists a large positive vertical wind shear around the cyclone between the upper (200 mb) and lower (900 mb) troposphere in the direction of storm motion, while the opposite occurs with a right-turning storm. Straight-moving cyclones do not show such a shear pattern. Statistical tests show that these results are significant at the 95% level or higher.

Tropospheric mean temperature fields around 13 tropical cyclone turning cases in the Atlantic and Pacific Oceans derived from the Nimbus 6 microwave sounder data during 1975 were also studied. Temperature gradients across these storms indicate (through the thermal wind relationship) vertical wind shear profiles similar to those obtained from the composite.

These results suggest or verify previous ideas that 1) by measuring certain parameters around a storm (sense of surrounding wind rotation, vertical wind shear between 200 and 900 mb, or gradient of tropospheric mean temperature) one may be able to make a better 24–36-h forecast of cyclone turning motion; 2) the turning motion of tropical cyclones is controlled by large-scale flow fields surrounding them; and 3) there seems to be a time lag between the changes in the environment and the response of the storm center to such changes.

### 1. Introduction

To predict the turning motion of tropical cyclones 24–36 h in advance is very difficult and quite often unsuccessful. Statistical prediction schemes (e.g., Hope and Neumann, 1970; Neumann and Lawrence, 1975) have great problems in forecasting such turning motion because of their strong emphasis on climatology and persistence. Numerical models also fail to predict cyclone turning motion most of the time. As a result, the largest tropical cyclone track forecast errors<sup>1</sup> are usually associated with storms undergoing a turn.

A detailed study of the characteristics of the surrounding environment of cyclones undergoing turning motion may give insight into ways of devising new schemes which may reduce forecast errors associated with turning motion. This paper presents

information on the environmental flow patterns around tropical cyclones prior to and at the time when these storms undergo turning motion. It will be shown that significant differences in the large-scale surrounding wind fields exist at 500 mb, and also at 200 and 900 mb levels between left-turning, straight-moving and right-turning storms. Temperature sounding data from the Nimbus 6 Scanning Microwave Spectrometer also provide evidence of some of these differences.

### 2. Forecast errors associated with turning motion

To examine this forecast problem more closely, a special study of tropical cyclone forecast errors occurring in the West Indies during the period 1961–77 was made.

#### *a. Selection of cyclone tracks*

The data sample consists of tropical cyclones in the West Indies west of 55°W with maximum sustained winds  $\geq 18 \text{ m s}^{-1}$ . The direction of

<sup>1</sup> Present affiliation: Laboratory for Atmospheric Research, University of Illinois at Urbana-Champaign, Urbana 61801.

<sup>1</sup> Forecast error is defined as the deviation of the forecast position of a tropical cyclone from its best-track verifying position.

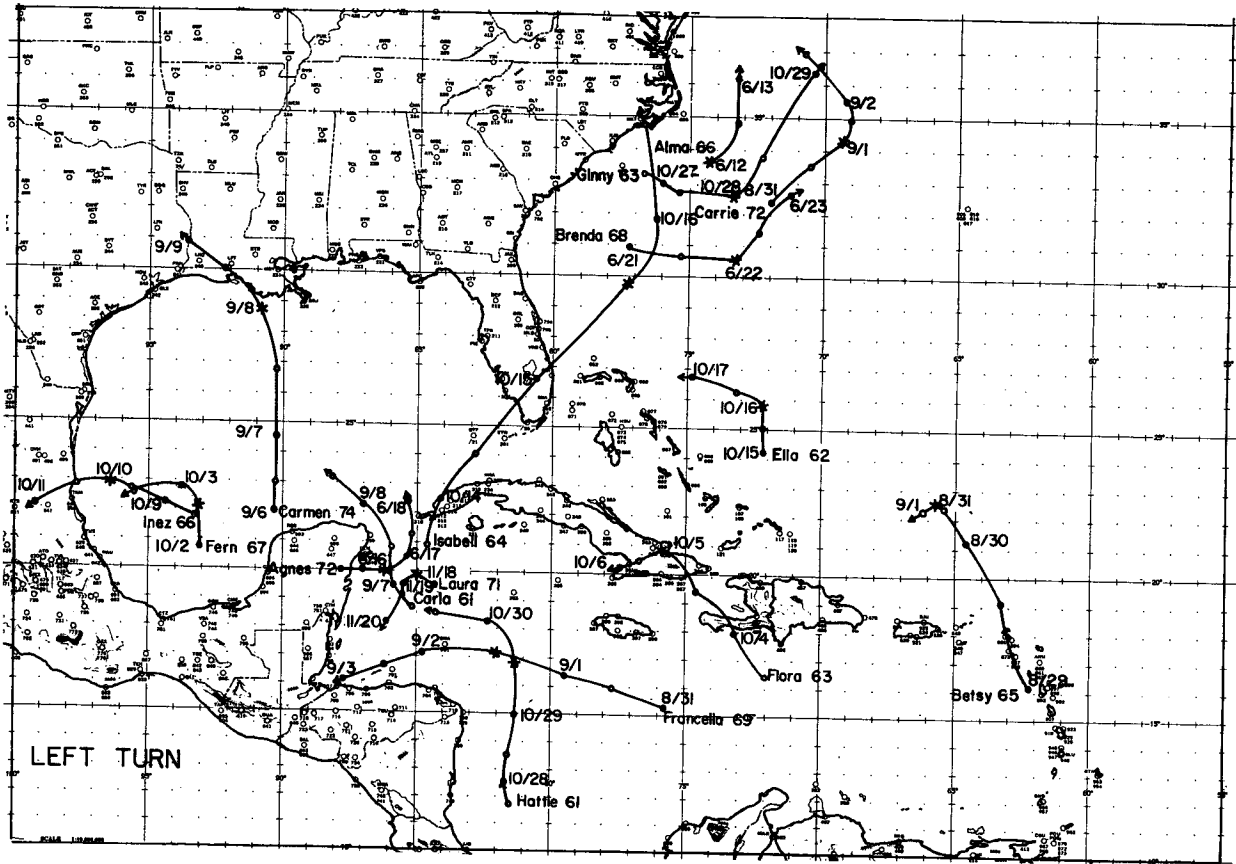


FIG. 1. Tracks of tropical cyclones used in this study which made a left turn. The asterisk on each track indicates the turn time T. The solid circle is the 0000 GMT position (with the date next to it) and the open circle is the 1200 GMT position.

motion (D) of each storm at a standard time T in hours (0000 or 1200 GMT) is defined as D(T). Three turn classes were then chosen according to the following criteria:

Left-turning:  $D(T + 12) - D(T) < -20^\circ$

Straight-moving:  $-10^\circ < D(T + 12) - D(T - 12) < 10^\circ$

Right-turning:  $D(T + 12) - D(T) > 20^\circ$ .

The time T was then defined as the turn time. In this way, 16 left-turning, 33 straight-moving and 28 right-turning cases were chosen. Tracks of these storms are shown in Figs. 1, 2 and 3.

*b. Forecast errors of sample storms*

The 24 h National Hurricane Center (NHC) official forecast errors issued for each storm at three time periods [24 h before turn time (T - 24), the turn time (T) and 24 h after turn time (T + 24)] were analyzed. Table 1 gives the average result for each turn class. The "special right turn" category consisted of cases where the average 24 h forecast error was greater than 350 km. It can be seen that a

considerable jump in the forecast error occurs at turn time in comparison with the forecast error for straight-moving cyclones. The forecast errors are even larger for 16 of the 22 special right-turn cases, jumping from 148 km before the turn to 417 km at turn time.

Fig. 4 shows the scatter of 24 h forecast positions made at turn time and the corresponding verifying positions for each turn class. Table 2

TABLE 1. Average 24 h official tropical cyclone track forecast errors (km) issued by the National Hurricane Center, Miami. T is the time when the storm starts to turn. See text for further explanation of turn classification. Note that the number of analyzed cases are different from those mentioned in Section 2a because forecast errors for some cases are not available.

Turn classification	24-h Forecast error (km) for forecasts issued at the following times		
	T - 24	T	T + 24
Left turn (10 cases)	235	289	206
Straight (23 cases)	148	169	196
Right turn (22 cases)	178	324	239
Special right turn (16 cases)	148	417	245



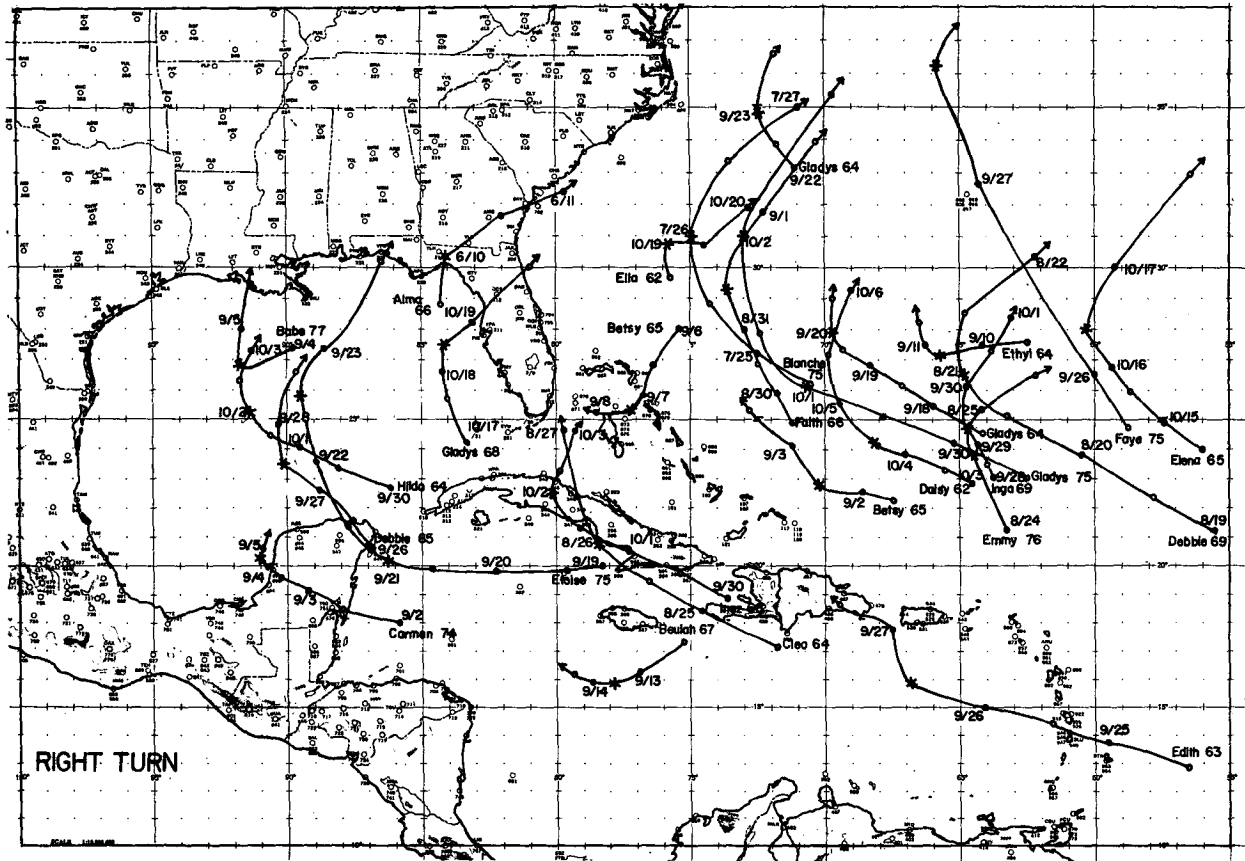


FIG. 3. As in Fig. 1 except for right-turning tropical cyclones.

conclusions to be drawn about the "average" differences in the surrounding environment between different data sets. Compositing tends to suppress random data noise and isolates mean characteristics common to each composite class. Differences be-

tween turning classes (if present) will give hints to forecasters as to which surrounding cyclone parameters to monitor in individual cases.

For each turn classification in Section 2a rawinsonde data at the following time periods were

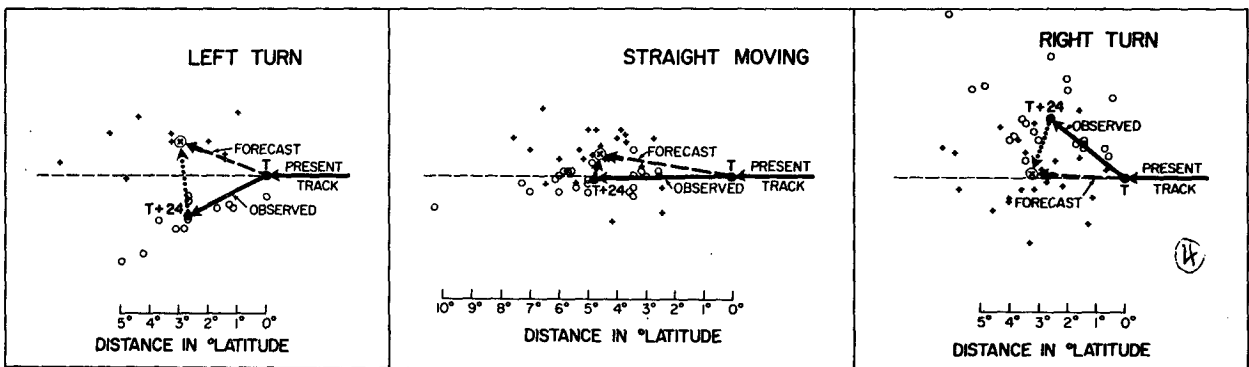


FIG. 4. National Hurricane Center 24 h forecast positions (denoted by +) made at the turn time for individual storms in each class and their actual positions (denoted by open circles) at the time T + 24. The ⊗ is the mean forecast position. The dashed arrow is the 24 h mean forecast track. The solid arrow from T to T + 24 is the mean distance (and direction) the storm has traveled during the 24 h. The dotted arrow indicates the average displacement of the forecast position from the actual position.

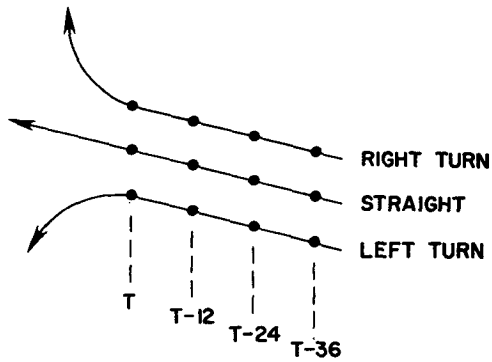


FIG. 5. Idealized picture of the three turn classes of tropical cyclones and of the time periods prior to turn which were composited.

composited: when the storm starts to turn (turn time, T), and 12, 24 and 36 h before turn time (T - 12, T - 24 and T - 36 respectively), as shown schematically in Fig. 5. Rawinsonde stations used in the data compositing are shown in Fig. 5.

Compositing is performed on a 15° latitude radius<sup>2</sup> cylindrical grid consisting of eight octants and eight radial bands, as shown in Fig. 7. The center of the grid corresponds to the storm center. The grid is rotated so that octant 1 is aligned along the direction of storm motion. See George and Gray (1976) for a more detailed description.

<sup>2</sup> Hereafter, all distances are referred to in degrees latitude (1° latitude = 111.1 km).

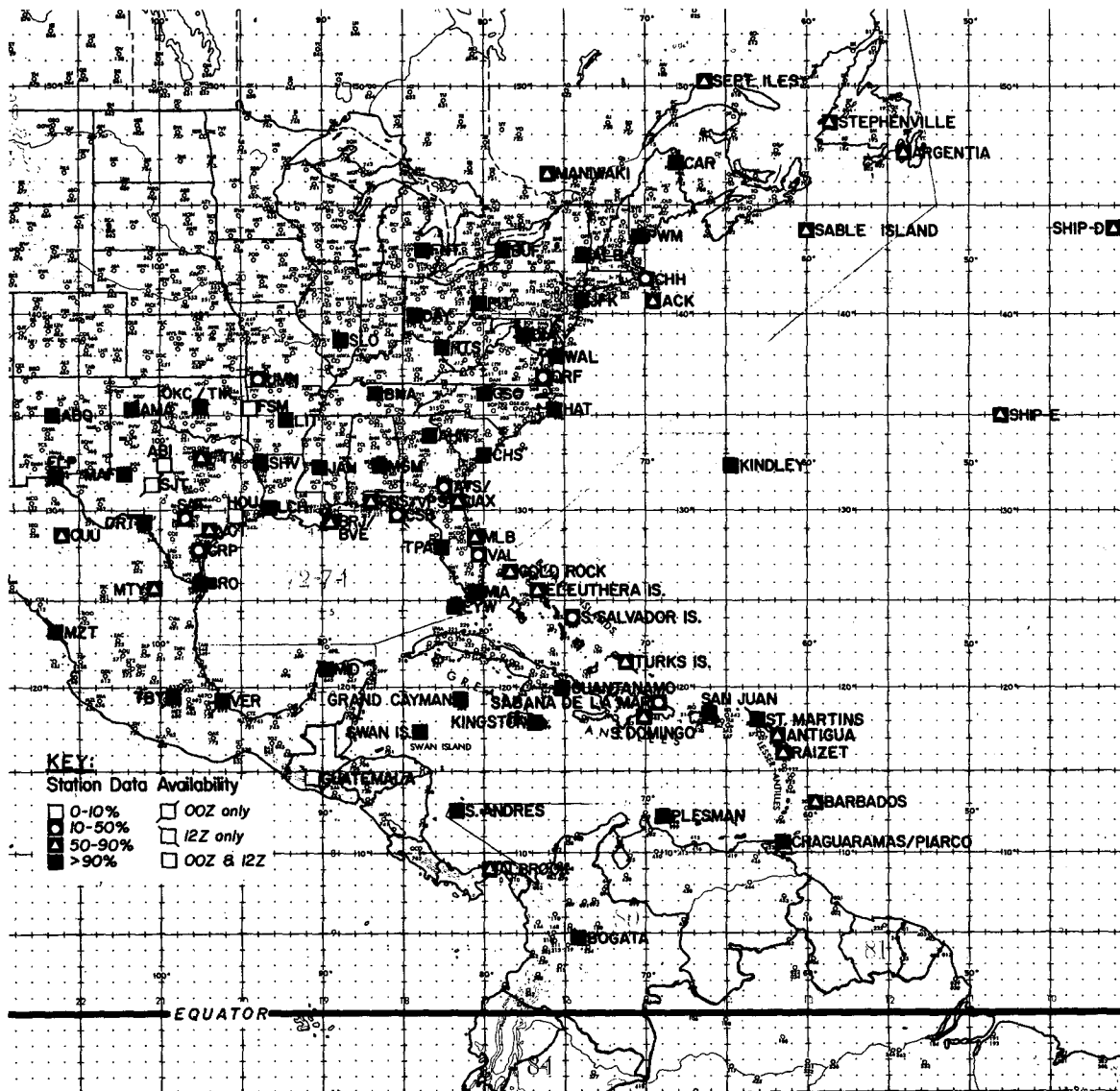


FIG. 6. Northwest Atlantic rawinsonde data network.

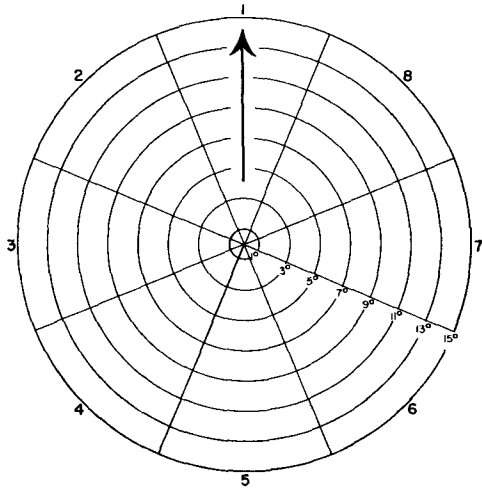


FIG. 7. Grid used for composing rawinsonde data. The arrow points in the direction of storm motion. Outer numbers denote octants. Numbers inside grid indicate distances from the center in degrees latitude.

Each wind vector is resolved into two components, one parallel to the direction of storm motion ( $V_P$ ) and one normal to it ( $V_N$ ), as shown in Fig. 8. All wind observations falling within a particular octant and radial band are averaged to give the composite  $V_P$  and  $V_N$  within that sector. These types of rawinsonde averaging processes are described in greater detail by Frank (1977).

**4. Surrounding flow at turn time**

It has been known for many years that tropical cyclone motion is well related to mid-tropospheric surrounding wind patterns. In a composite study of tropical cyclone motion stratified according to direction, latitude, speed, intensity and intensity change, George and Gray (1976) found that 500 mb is the best steering level for direction and 700 mb is the best for

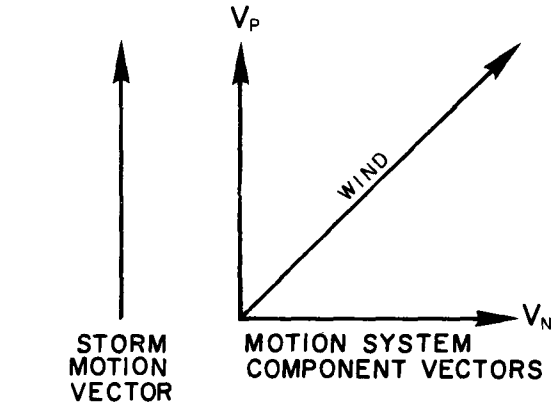


FIG. 8. Parallel ( $V_P$ ) and perpendicular ( $V_N$ ) components of a wind vector showing their relation to the storm motion vector.

cyclone speed. To better refine the present knowledge of the steering flow associated with cyclones undergoing turning motion, composite flow fields at 900, 700, 500 and 200 mb at turn time were analyzed. Although 500 mb is found to be the best steering level, flow fields at the upper (200 mb) and lower (900 mb) tropospheric levels also appear quite useful.

*a. Flow field at 500 mb*

Fig. 9 shows the composited 500 mb streamline patterns at turn time for the three turning classes. The flow field ahead of the storm can be seen to be a very good indicator of current directional change.

The  $V_N$  components of the winds at 500 mb in the front and back octants are shown in Fig. 10. The number next to each arrow indicates the magnitude of the  $V_N$  component ( $m s^{-1}$ ) averaged between  $5-11^\circ$  radius. For each classification, if a weighted average of  $V_N$  in the front three and back three octants [ $V_N$  in octants 1 (front) and 5 (back) are given a

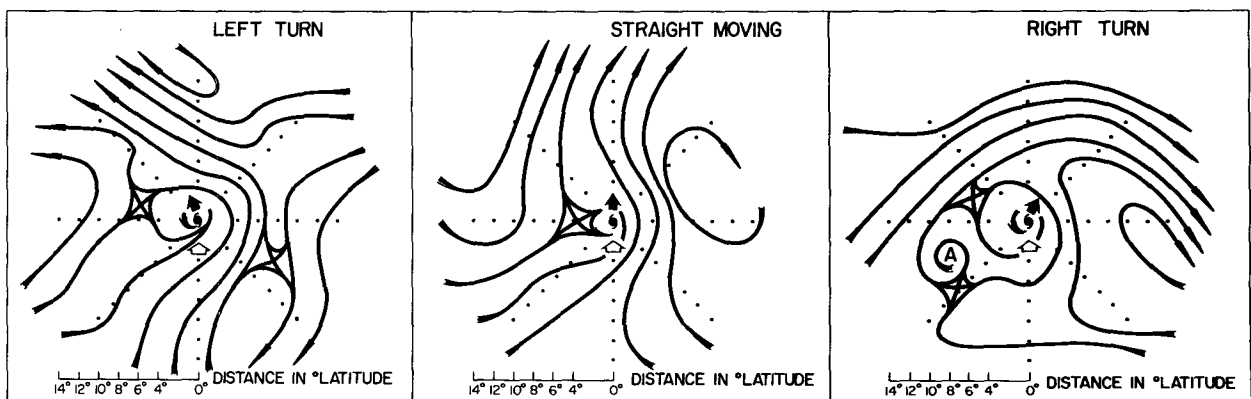


FIG. 9. 500 mb streamlines for the three turn classes at turn time. Open arrows indicate the instantaneous direction of storm motion. Solid arrows indicate the movement of the storm during the next 12 h.

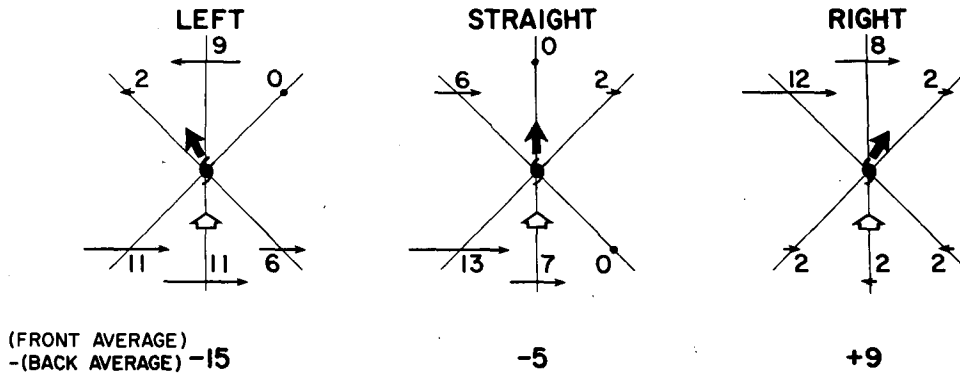


FIG. 10. Sum of  $V_N$  [wind component ( $m s^{-1}$ ) normal to direction of storm motion] at 500 mb within  $5-11^\circ$  radii from the storm center in various octants at the turn time  $T$ . The length of the arrow is proportional to the magnitude of the wind. See text for description of the averaging process. Open arrows indicate the instantaneous direction of storm motion and solid arrows the movement of the storm during the next 12 h.

weight of 1 and those in the right and left octants a weight of 0.5] is calculated, the front octant average minus the back octant average will give a horizontal  $V_N$  shear value. This is shown at the bottom of the figure. These shear values are significantly different between the three turn classes and they well infer turning motion at turn time.

With decreasing oceanic middle level rawinsonde and propeller aircraft data, such 500 mb level information on individual cyclone cases is usually not available. Since upper and lower tropospheric wind data are becoming more available with time from satellite and jet aircraft observations it may be more useful to try to establish steering flow relationships at upper and lower tropospheric levels.

*b. Upper and lower tropospheric flow*

The  $5-11^\circ$  radius average of the front and back octants  $V_N$  (200 mb) and  $V_N$  (900 mb) for the three turn classes at turn time is shown in Fig. 11. The differences in horizontal  $V_N$  shear values between

turn classes follow the same trend as those at 500 mb. Thus, it seems possible to use the average 200 and 900 mb winds to infer turning motion at turn time.

**5. Surrounding flow before turn time**

A study of the composite  $V_N$  flow fields 24 or 36 h before turn time at various levels reveals no significant differences between the turn classes. The  $V_P$  component of the wind at 500 mb and the upper (200 mb) and lower (900 mb) troposphere, however, shows important relationships with cyclone turning motion 24-36 h before it takes place.

*a. 500 mb flow*

The  $V_P$  components of the winds (parallel to the direction of storm motion) at 500 mb in the front left (2), back left (4), back right (6) and front right (8) octants are found to best correlate with turning motion 24-36 h before turn time. These components

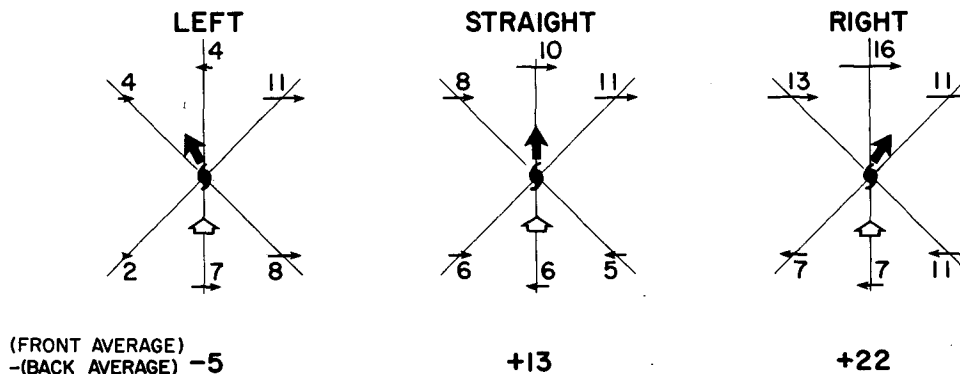


FIG. 11. As in Fig. 10 except  $V_N$  is the sum of the average winds between 200 and 900 mb at the turn time ( $T$ ).

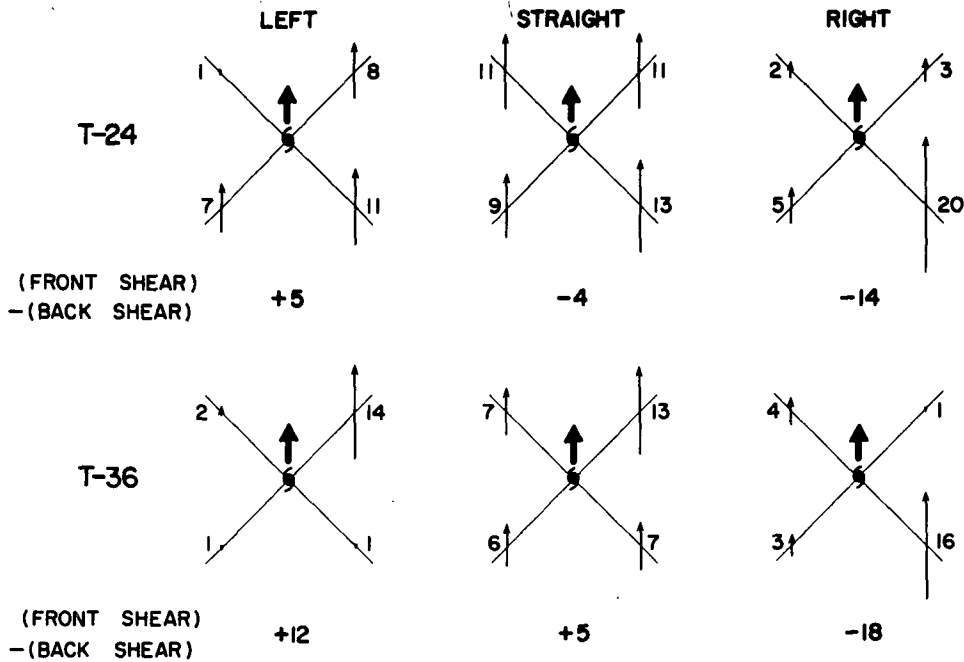


FIG. 12. Sum of 500 mb  $V_p$  [wind component ( $m s^{-1}$ ) parallel to direction of storm motion] within  $5-11^\circ$  radii from the storm center in octants 2, 4, 6 and 8 for the three turn classes at 24 h ( $T - 24$ ) and 36 h ( $T - 36$ ) before turn time. The heavy arrow indicates the direction of storm motion. See text for description of calculating the front and back shear.

are shown in Fig. 12. At 24 h before turn time ( $T - 24$ ), there exists at the front of the storm a strong cyclonic shear of  $V_p$  [ $V_p(\text{right}) - V_p(\text{left})$ ] for the left-turning storms. This shear is denoted by  $\Delta V_p / \Delta n$ , where  $\Delta n$  represents the distance between octants 2 and 8 or 4 and 6. This front  $V_p$  shear is about zero for the other two turn classes. Behind the cyclone, the right minus left  $V_p$  shear is cyclonic for all three classes. The magnitude of this  $V_p$  shear is largest for right-turning storms. Subtracting the  $V_p$  right minus left shear behind the storm from that in front of the storm, that is,  $[(V_{p_8} - V_{p_2}) / \Delta n - (V_{p_6} - V_{p_4}) / \Delta n]$ , where the numeric subscripts denote octant numbers, a front minus back  $V_p$  shear can be obtained which might be used to identify turning motion 24 h before it takes place: a positive value for left-turning, small negative for straight-moving and large negative value for right-turning.

At 36 h before turn time ( $T - 36$ ) a similar difference in the front minus back  $V_p$  shear exists between the three turn classes, as indicated in the lower half of Fig. 12. Notice that the front minus back  $V_p$  shear for straight-moving storms at  $T - 36$  is the same as that for left-turning storms at  $T - 24$ . This appears to reduce the distinguishing power of this shear to forecast turning. However, given the current low skill of forecasting turning motion, this 500 mb shear information may still be useful.

If aircraft reconnaissance flights were available to better measure these middle-level outer radius

shear patterns, then an improvement in forecasting turning motion might result. Such aircraft reconnaissance requires special propeller aircraft capability and will likely be unavailable in many or most cyclone forecast situations. By contrast, satellite-derived winds in the upper and lower troposphere should be more easily available.

*b. Upper and lower tropospheric flow*

The component of the 200–900 mb vertical wind shear parallel to the direction of storm motion 24–36 h before turn time is significantly different between the three turn categories.

Fig. 13 shows the average  $V_p$  wind within  $7-11^\circ$  radius<sup>3</sup> from the storm center in octants 1 (front) and 5 (back) at 200 and 900 mb 24 h before the turn time ( $T - 24$ ). In front of the storm, right-turning cyclones show a large negative wind shear between these two levels [ $V_p(200 \text{ mb}) - V_p(900 \text{ mb})$ ] while both left-turning and straight-moving storms have positive wind shear values. Behind the storm, the vertical wind shear is negative for straight-moving

<sup>3</sup> The reasons for using  $7-11^\circ$  are twofold: 1) since this flow is related to directional change of the storm 24–36 h ahead, one would expect this relation to be more significant further out from the storm center, where the environmental steering flow influences are much more dominant than that of the storm, and 2) the value of  $V_p$  in this radial band correlates best with the directional change of the storm.

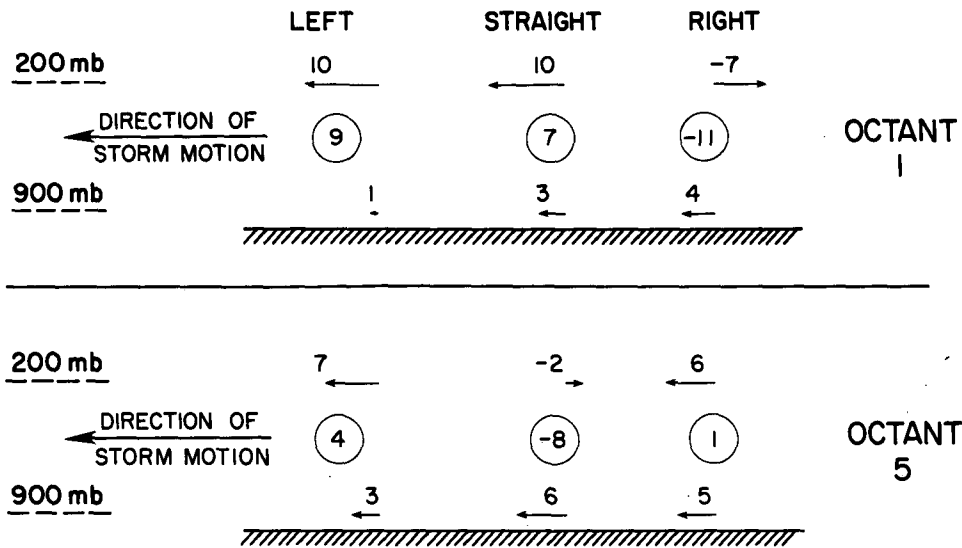


FIG. 13. Cross-sectional view of the average  $V_p$  wind components ( $m s^{-1}$ ) at 200 and 900 mb within  $7-11^\circ$  radii from the storm center in octants 1 and 5 24 h before turn time ( $T - 24$ ). The circled numbers are the values of the vertical wind shear [ $V_p(200\text{ mb}) - V_p(900\text{ mb})$ ].

storms and slightly positive for the other two turn classes. The average front and back vertical wind shears in the direction of storm motion are 7, -1 and  $-6 m s^{-1}$  for left-, straight- and right-moving cyclones, respectively. The same shear values at  $T - 36$  are 3, 0 and  $-10 m s^{-1}$  (see Fig. 14). Thus, for left-turning storms the net vertical wind shear in the direction of storm motion in octants 1 (front) and 5 (back) is positive. The shear is about zero

for a straight-moving storm and negative for a right-turning storm.

Such differences in tropospheric vertical wind shear between the turn classes only exist 24 and 36 h prior to turn time (Fig. 15). This shear difference does not show up as the storm approaches its turn time. Wind shear values at  $T - 48$  and before cannot be obtained because of the lack of cases.

Thus, if one is able to obtain winds in the upper

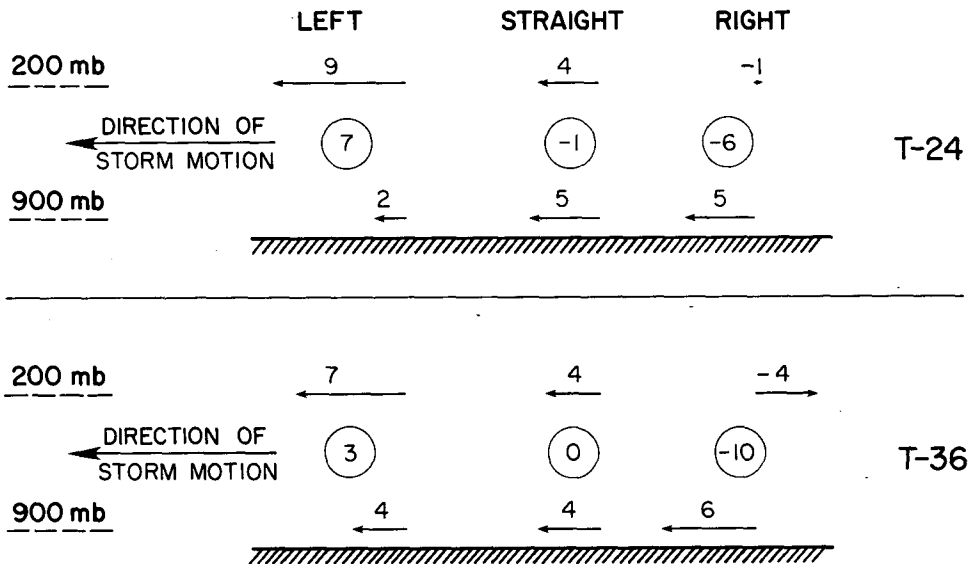


FIG. 14. Cross-sectional view of the sum of average  $V_p$  wind components ( $m s^{-1}$ ) within  $7-11^\circ$  radii from the storm center in octants 1 and 5 at 200 and 900 mb at 24 h ( $T - 24$ ) and 36 h ( $T - 36$ ) before turn time for the three turn classes. The circled numbers are the values of the vertical wind shear [ $V_p(200\text{ mb}) - V_p(900\text{ mb})$ ].

and lower troposphere around a storm (for example, from satellite observations), it may be possible to better anticipate cyclone turning motion 24–36 h before it takes place.

*c. Individual case analysis*

To see how valid the composite results are for individual turning storms, the  $V_p$  vertical shear described in the previous section for individual cases in the sample was also studied. Individual case analysis is severely handicapped by data availability. Wind and height data must be interpolated from analyzed weather maps. Nevertheless, an attempt was made to evaluate this vertical shear parameter [ $V_p(200\text{ mb}) - V_p(900\text{ mb})$ ] for individual turning situations. The 200 mb winds were estimated from the height contours, using the geostrophic wind relationship. If there were no contour maps an estimate was made from the 200 mb streamline analysis. If neither was available, the case was not analyzed. The 900 mb winds were estimated from either the 3000 ft PIBAL maps or from the NHC ATOLL (top of the Ekman Layer) maps. If neither was available, an estimate was made from surface pressure maps, again using the geostrophic wind relationship. These methods restricted the analysis of the  $V_p$  vertical wind shear to only about two-thirds of the individual cases in the sample.

Fig. 16 shows the shear values obtained at both  $T - 24$  and  $T - 36$ . Although there is a large spread in the vertical wind shear for each classification (which is to be expected because of the inherent data uncertainties) a relationship between the verti-

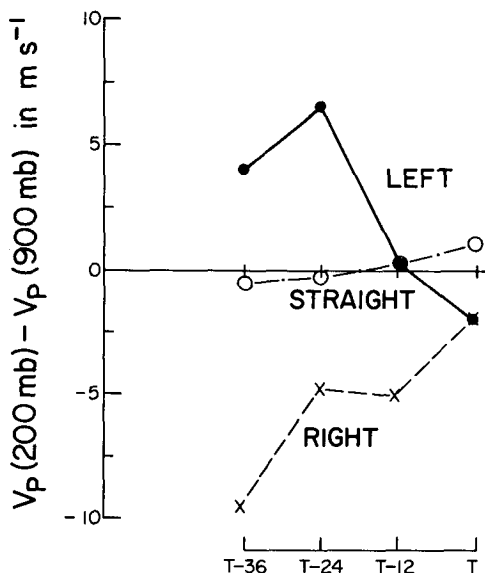


FIG. 15. Vertical wind shear for different time periods. The ordinate is the value of the average vertical wind shear ( $\text{m s}^{-1}$ ) within  $7\text{--}11^\circ$  radii from the storm center in octants 1 and 5.

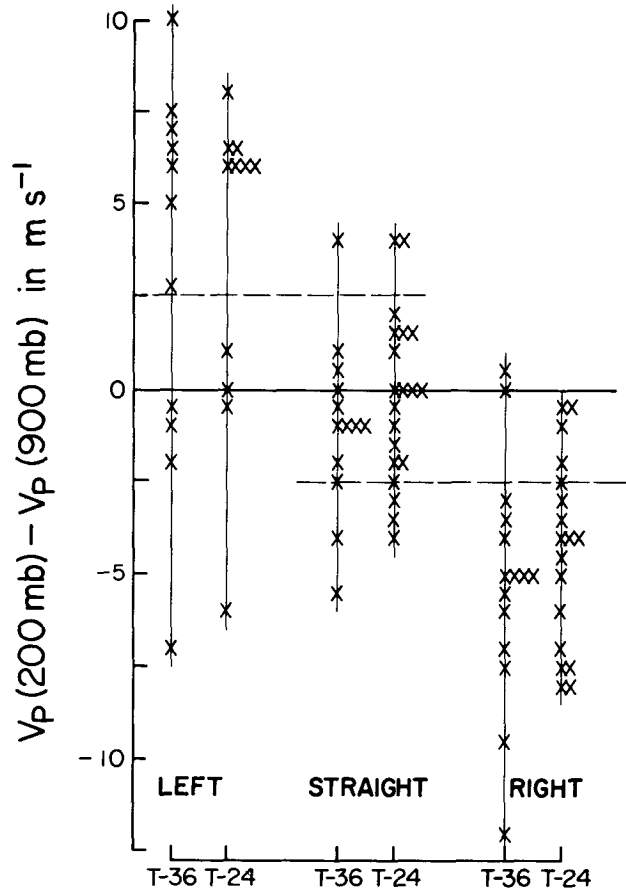


FIG. 16. Vertical wind shear between 200 and 900 mb at  $T - 24$  and  $T - 36$  time periods for individual storms. The ordinate is the same as in Fig. 15. Each cross represents the wind shear value from one individual storm. Equal values of the wind shear are plotted next to each other. The dashed lines indicate the threshold values described in the text.

cal wind shear and the turning motion, similar to the one in the composite, does show up.

To make sure that the results for these individual cases are not due to random chance, a  $t$  test was performed on the three samples of individual storms. The results for both  $T - 24$  and  $T - 36$  are shown in Table 3. The symbols are defined as follows:

- $N$  number of cases in which the vertical wind shear parameter can be estimated
- $\bar{x}$  sample mean vertical wind shear
- $\mu$  average vertical wind shear of all three categories of storms from composite data (assumed to be the population mean)
- $s$  standard deviation of the sample
- $t(95\%)$  value of  $t$  at 95% significance level given in Panofsky and Brier (1958).

It is seen that the mean vertical wind shears for both the left- and right-turning cases are significant at the 95% level. This lends confidence to the

TABLE 3. The  $t$  test of the vertical wind shear parameter on the three samples of individual storms for both T - 24 and T - 36. Symbols are defined in the text.

Turn classification	$N$	$\bar{x}$	$\mu$	$s$	$t =  \bar{x} - \mu (N - 1)^{1/2} s^{-1}$	$t(95\%)$
T - 24						
Left-turning	11	7.18	0	8.67	2.62	2.23
Straight-moving	20	-0.45	0	4.54	0.43	2.09
Right-turning	18	-8.72	0	5.07	7.09	2.11
T - 36						
Left-turning	11	6.23	-2.33	10.27	2.64	2.23
Straight-moving	14	-1.71	-2.33	4.60	0.49	2.16
Right-turning	15	-10.33	-2.33	6.39	4.68	2.15

conclusion that tropospheric vertical wind shear can be used as an indicator of turning motion 24–36 h before such motion occurs.

If we set threshold values for the 200–900 mb  $V_p$  vertical wind shear as

$$\begin{aligned} >5, & \text{ Left turn} \\ -5 \text{ to } 5, & \text{ Straight} \\ < -5, & \text{ Right turn} \end{aligned}$$

it is found that 64% of the left-turning storms have vertical wind shears  $> 5$  for both T - 24 and T - 36 time periods. For the straight-moving storms, 77% occurred within the range at T - 36 and 75% at T - 24. For the right-turning storms 87% have vertical wind shears  $< -5$  at T - 36 and 72% at T - 24. The present level of success in forecasting turning motion is considered to be significantly less than this, as evident from the scatter of forecast points shown in Fig. 4.

Since the techniques in deriving lower and upper tropospheric winds from (geostationary) satellite observations are improving, the information on such vertical wind shear should become more available as time goes on and there may be hope for an improvement in future turning motion forecasts.

## 6. Study of satellite temperature sounding data

The vertical wind shear structure described in Section 5 should be related through the thermal wind relationship to the mean tropospheric temperature differences across these storms. An estimate of the magnitude of the temperature gradient can be obtained from the thermal wind equation

$$\frac{\Delta T}{\Delta n} \approx \frac{f}{R} \left[ \ln \left( \frac{p_1}{p_2} \right) \right]^{-1} V_T, \quad (1)$$

where  $\Delta n$  is the horizontal distance across which a temperature difference  $\Delta T$  is measured,  $V_T$  is the thermal wind, or in this case,  $V_p(200 \text{ mb}) - V_p(900 \text{ mb})$ ,  $p_1 = 900 \text{ mb}$ ,  $p_2 = 200 \text{ mb}$ ,  $f$  is the Coriolis parameter and  $R$  the gas constant. If we assume  $f$  to be  $5 \times 10^{-5} \text{ s}^{-1}$  (corresponding to  $20^\circ \text{N}$ ) and

$\Delta n = 18^\circ$  latitude, then for a vertical wind shear of  $10 \text{ m s}^{-1}$ ,  $\Delta T \approx 2.2 \text{ K}$ .

To investigate the existence of such a horizontal temperature gradient, temperature sounding data from the Nimbus 6 Scanning Microwave Spectrometer (SCAMS) of 1975 were examined. Since this sounder can resolve tropospheric temperature gradients of the above magnitude, we should expect the sounder data to be able to help specify turning motion.

### a. The Scanning Microwave Spectrometer

The SCAMS on board the Nimbus 6 polar-orbiting satellite is a five-channel instrument sensing radiation nominally at 22.235, 31.65, 52.85, 53.85 and 55.45 GHz (Staelin *et al.*, 1975a). The latter three frequencies are used for sounding the atmosphere, while the first two are used to infer vertically integrated atmospheric water vapor and liquid water content. The Nimbus 6 spacecraft is in a sun-synchronous (1130 and 2230 Local Time) near-polar orbit at an altitude of approximately 1100 km. The SCAMS instrument scans across the spacecraft track in 13 steps at increments of  $7.2^\circ$  in the scan angle each 16 s which results in a spatial resolution of 145 km near nadir, degrading to 200 km down-track by 360 km cross-track at the maximum scan angle (Staelin *et al.*, 1975a). Approximately 400 individual soundings can be obtained within  $15^\circ$  of the center of a tropical cyclone for each 12 h period.

### b. Tropical cyclones analyzed

A total of 13 cases<sup>4</sup> (11 individual storms) in both the Pacific (northeast and northwest) and Atlantic Oceans during 1975 were examined. As explained in Section 2a, only cyclones with maximum sustained wind  $\geq 18.0 \text{ m s}^{-1}$  were included. The tracks for these storms are shown in Fig. 17. The distribution of storms in each turn class is given in Table 4. Satellite data were categorized by time (T, T - 12,

<sup>4</sup> This is all the SCAMS information available to the authors at this time.



TABLE 4. Distribution of turn cases in the Atlantic and Pacific Oceans used in studying satellite temperature sounding data around tropical cyclones.

Ocean	Left	Straight	Right
Atlantic (West Indies)	0	2	4
Northwest Pacific	1	1	3
Northeast Pacific	1	1	0
Total	2	4	7

$T - 24$  and  $T - 36$ ) as described in Section 3. The mean 1000–250 mb temperatures around each storm for each time period were derived from the brightness temperatures (the raw data obtained from the sounder) as described in Waters *et al.* (1975). The same method used in the rawinsonde composite was employed (see Section 3) to obtain average layer mean temperature at each of the grid points in Fig. 7 for each storm. To minimize contamination by precipitation, data points with integrated liquid water contents  $\geq 0.5 \text{ kg m}^{-2}$  were not used in the averaging process. According to Staelin *et al.* (1975b) this should eliminate most of the contaminated data.

The accuracy of atmospheric temperatures derived from satellite sounders is a pertinent point. Data from a microwave sounder were used because microwave soundings are unaffected by non-raining clouds (Staelin *et al.*, 1975b). The extensive cloudiness near tropical cyclones precludes the exclusive use of infrared sounding data. When the 1000–250 mb layer mean temperature at a single spot is compared with the nearest grid point data analyzed by the National Meteorological Center (NMC) the root-mean-square difference is  $\sim 2 \text{ K}$  (Landsat/Nimbus Project, 1976). *It must be remembered, however, that only temperature difference and not absolute temperature is a requirement for the wind shear determination.* In addition, each grid point

value is an average of a considerable number of observation points, and precipitation-contaminated data points have been eliminated. The satellite-derived temperature differences obtained in the way described above should therefore be accurate to within a few tenths kelvin (Staelin *et al.*, 1975b).

### c. 1000–250 mb mean temperature fields

For convenience, the 1000–250 mb layer mean temperatures were analyzed in the following way. All layer-mean temperatures at grid points within  $5\text{--}15^\circ$  radius<sup>5</sup> from the storm center were averaged to obtain an average layer-mean temperature  $\bar{T}$ . The deviation of each grid point temperature from  $\bar{T}$  was calculated (for all points in the grid). These deviations were used for the analysis instead of the absolute values. An example of the temperature deviation field for three individual cases 24 h before turn time (one in each turn class) is shown in Fig. 18. This figure shows the typical expected difference in temperature structure existing between a left-turning, straight-moving and right-turning storm as implied by the difference in vertical wind shear structure discussed in Section 5. The left-turning storm shows a temperature gradient across the storm corresponding to a thermal wind, or vertical wind shear, in the direction of storm motion while the opposite occurs for the right-turning storm. There is very little temperature gradient for the straight-moving case. An examination of the other cases indicates that the temperature gradients of most significance exist in front of the storm. In addition, for most of the left- and right-turn cases studied, there exists a region where the troposphere

<sup>5</sup> The reasons for using  $5\text{--}15^\circ$  are 1) more data are available outside  $5^\circ$  (a lot of data were eliminated within  $5^\circ$  because of high liquid water content), and 2)  $15^\circ$  is the outermost radius used in the rawinsonde composite study.

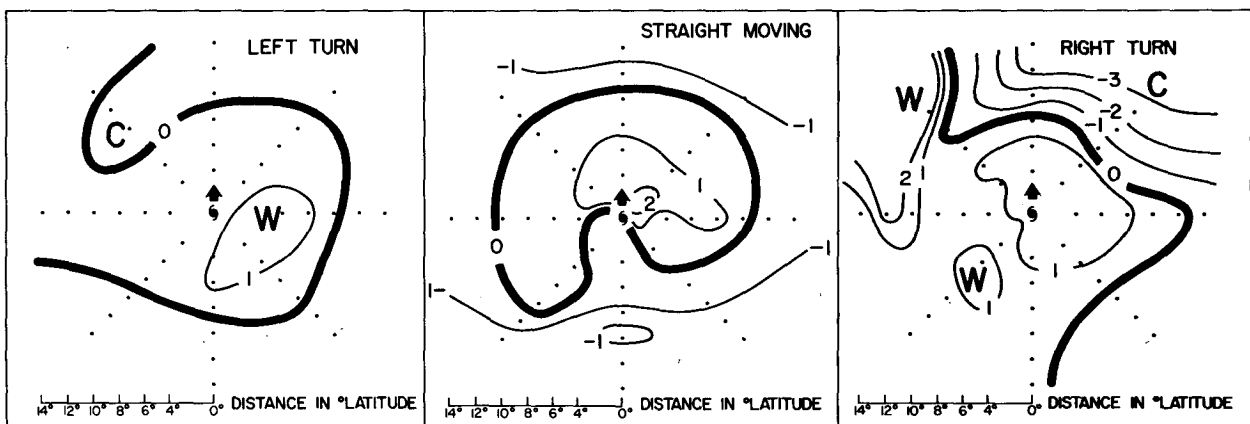


FIG. 18. 1000 to 250 mb layer mean temperature deviation from 5 to  $15^\circ$  radii average mean temperature derived from the Nimbus 6 SCAMS temperature sounding data 24 h before turn time. The arrow from the storm center indicates the direction of storm motion.

TABLE 5. The 1000–250 mb layer mean temperature deviations from 5–15° radii average in octants 2 (left front) and 8 (right front) within 9–13° radius from the storm center for various storms in the North Pacific and Atlantic Oceans 24 h before turn time. Vertical wind shear in the direction in which the storm is going is calculated from the thermal wind relationship using a horizontal distance of 18°. The Coriolis force  $f$  is taken to be  $5 \times 10^{-5} \text{ s}^{-1}$ .

Storm	Region	Octant 2	Octant 8	Octant 2 minus Octant 8	Corresponding vertical wind shear ( $\text{m s}^{-1}$ )	Turn
Phyllis	west Pacific	-0.8	0.2	-1.0	4.5	left
Ilsa	east Pacific	-0.9	1.5	-2.4	10.9	left
Alice	west Pacific	-0.7	0.0	-0.7	3.2	straight
Lily	east Pacific	-0.6	-0.1	-0.5	2.3	straight
Eloise	west Atlantic	0.2	0.2	0.0	0.0	straight
Caroline	west Atlantic	-1.1	2.9	-4.0	18.2	straight
Eloise	west Atlantic	1.5	-0.2	1.7	-7.7	right
Eloise	west Atlantic	1.6	-2.0	3.6	-16.4	right
Gladys	west Atlantic	0.1	-1.4	1.5	-6.8	right
Faye	west Atlantic	0.3	-0.4	0.7	-3.2	right
June	west Pacific	0.7	-1.6	2.3	-10.5	right
Tess	west Pacific	-0.7	-1.9	1.2	-5.5	right
Cora	west Pacific	1.0	1.0	0.0	0.0	right

is relatively cold in the direction toward which the storm is moving, as indicated in the examples given in Fig. 18.

To describe these temperature gradients in more quantitative terms, temperature deviations at 9–13° radius<sup>6</sup> in octants 2 (left front) and 8 (right front) for all cases were studied. Results are shown in Table 5. Both left-turning cases show that the mean tropospheric temperature is lower to the left front of the storm. For the straight-moving storms, only Caroline shows a large negative tropospheric shear. The reason for this is unknown. However, all other straight-moving cases show only a very weak temperature gradient across the front of the storm. In addition, all three cases show a region of cold air in octant 1 (not shown). Of the seven right-turning storms, only Cora shows no temperature gradient. The others indicate a relatively cold troposphere to the right front of the storm.

These results were obtained, as described earlier, after elimination of data points with integrated liquid water content  $\geq 0.5 \text{ kg m}^{-2}$ . To see if this process is of any great significance, temperature deviation fields without eliminating any data were also analyzed. A comparison between the two sets of results shows very little difference in the temperature structure and temperature gradients at large radii from the storm center. It would appear that it is not necessary to eliminate those data points with appreciable liquid water content provided temperatures at large distances from the storm center are used.

<sup>6</sup> In order to obtain the horizontal temperature gradient normal to  $V_p$  in octant 1, at radii 7–11° (the area where the vertical wind shear parameter is of significance), one has to consider temperatures in octants 2 and 8 at radii 9–13° (see Fig. 7).

These results suggest that very pertinent information on forecasting tropical cyclone turning motion 24 h in advance may be obtained from satellite sounder information in regions devoid of rawinsonde, aircraft and clouds for satellite wind vector determination. Newer and better satellite sounders are likely to be available in the future for even better determinations.

## 6. Summary and recommendations

The results of this study indicate that there are parameters in the large-scale environment around tropical cyclones at upper and lower tropospheric levels (in addition to the previously considered crucial middle level) which can provide information about their turning motion 24–36 h before it occurs. An estimate of the  $V_N$  component of the winds at 200 and 900 mb at 5–11° radius around the storm from satellite observations may also be useful for making short-range (0–12 h) forecasts of turning motion. Of greater significance is the possibility of using the  $V_p$  vertical wind shear to specify turning motion 24–36 h in advance. The fact that favorable environmental conditions are evident 24–36 h prior to turn time indicates that there is likely a time lag between changes in the environmental flow parameters surrounding a storm and the response of the storm to such changes.

At certain times it may not be possible to derive satellite winds at 900 and 200 mb because of an extensive cirrus canopy or because upper-level cloud motions are lacking. In these cases the satellite sounder, with its tropospheric temperature difference measurement capability, may be useful in augmenting missing wind data. Since contamination

of the sounding data by precipitation is negligible at large radii, the Microwave Sounding Unit (which does not have any water vapor channel) on board the TIROS-N satellite now in orbit might be used to monitor tropospheric temperature gradients across a storm to determine the upper and lower tropospheric vertical wind shear. It is suggested that temperature data obtained from such a sounder be used on an operational basis to test the applicability of these results.

With the large increase in computer technology and the development of more sophisticated cyclone forecast schemes, one would expect a continuous increase in tropical cyclone forecast skill. While this has been true on the average in the 1960's and early 1970's, tropical cyclone track 24 h forecast errors have been showing a slight increase in the last three to four years (see, e.g., Joint Typhoon Warning Center, 1977). These forecast error increases are likely a result of an over-reliance by the various forecast techniques on middle-level flow patterns, and a subsequent gradual reduction of oceanic rawinsonde and aircraft data to measure such flow patterns. Atlantic weather ships *Echo* and *Delta* were decommissioned in 1973. Very few oceanic propeller aircraft flights are now made. These changes have significantly reduced the already scanty mid-tropospheric Atlantic wind-height data. Accurate analysis of middle-level flow fields has always been difficult. At some locations and time periods it is now nearly impossible to obtain a meaningful analysis. Neumann (private communication) has discussed how NMC tropical analysis schemes can produce a quite unrepresentative middle-level steering current determination. He has documented cases in which an erroneous wind observation drastically changes middle-level computer-analyzed flow fields. This seriously affects the performance of tropical cyclone forecast models based on middle-level steering flow concepts (e.g., see Lawrence, 1979). New forecasting schemes (regardless of how sophisticated) which utilize middle-level flow patterns should encounter similar observational problems.

Because of the increasing availability of satellite-derived information at upper and lower tropospheric levels, it is suggested that research on storm motion be concentrated on studying the relationships between upper and lower tropospheric parameters and storm movement. The next steps in this research

will be to try to relate upper and lower level parameters with cyclone speed changes, stalling and looping motions, and other special cyclone motion characteristics.

*Acknowledgments.* The authors would like to thank Mr. Edwin Buzzell for his programming assistance and Mrs. Bonnie Weber and Mrs. Barbara Brumit for their help in manuscript preparation and part of data reduction.

This research was supported by a NHEML NOAA Research Grant NA 79 RAD 00002 with supplementary support from NASA Grant NSG-5258.

#### REFERENCES

- Frank, W. M., 1977: The structure and energetics of the tropical cyclone. I: Storm structure. *Mon. Wea. Rev.*, **105**, 1119-1135.
- George, J. E., and W. M. Gray, 1976: Tropical cyclone motion and surrounding parameter relationships. *J. Appl. Meteor.*, **15**, 1252-1264.
- Hope, J. R., and C. J. Neumann, 1970: An operational technique for relating the movement of existing tropical cyclones to past tracks. *Mon. Wea. Rev.*, **98**, 925-933.
- Joint Typhoon Warning Center, 1977: Annual typhoon report. U.S. Fleet Weather Center, Joint Typhoon Warning Center, Guam, COMNAVMARINAS, Box 17, FPO San Francisco 96630, 125 pp. [NTIS AD-A055].
- Landsat/Nimbus Project, 1976: *The Nimbus 6 Data Catalog*, Vol. 2. NASA/Goddard Space Flight Center, Greenbelt, MD, pp. 1-2 through 1-4 [NTIS N77-29688].
- Lawrence, M. B., 1979: Atlantic hurricane season for 1978. *Mon. Wea. Rev.*, **107**, 477-491.
- Neumann, C. J., and M. B. Lawrence, 1975: An operational experiment in the statistical-dynamical prediction of tropical cyclone motion. *Mon. Wea. Rev.*, **103**, 665-673.
- Panofsky, H. A., and G. W. Brier, 1958: *Some Applications of Statistics to Meteorology*. The Pennsylvania State University Press, 224 pp.
- Staelin, D. H., A. H. Barrett, P. W. Rosenkranz, F. T. Barath, E. J. Johnson, J. W. Waters, A. Wouters and W. B. Lenoir, 1975a: The scanning microwave spectrometer (SCAMS) experiment. *The Nimbus-6 User's Guide*, J. E. Sissala, Ed., LANDSAT/Nimbus Project, NASA/Goddard Space Flight Center, Greenbelt, MD, 59-86 [NTIS N76-31256].
- , A. L. Cassel, K. R. Kunzi, R. L. Pettyjohn, R. K. L. Poon and P. W. Rosenkranz, 1975b: Microwave atmospheric temperature sounding: Effects of clouds on the Nimbus 5 satellite data. *J. Atmos. Sci.*, **32**, 1970-1976.
- Waters, J. W., K. F. Kunzi, R. L. Pettyjohn, R. K. L. Poon and D. H. Staelin, 1975: Remote sensing of atmospheric temperature profiles with the Nimbus 5 microwave spectrometer. *J. Atmos. Sci.*, **32**, 1953-1969.
- Williams, K. T., and W. M. Gray, 1973: Statistical analysis of satellite-observed trade wind cloud clusters in the western North Pacific. *Tellus*, **25**, 313-336.